Acta Pharmaceutica Sinica B 2018;8(1):85–96

Chinese Pharmaceutical Association
Institute of Materia Medica, Chinese Academy of Medical Sciences

Acta Pharmaceutica Sinica B

www.elsevier.com/locate/apsb
www.sciencedirect.com

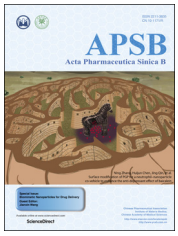

ORIGINAL ARTICLE

Substance P-modified human serum albumin nanoparticles loaded with paclitaxel for targeted therapy of glioma

Chunhui Ruan, Lisha Liu, Yifei Lu, Yu Zhang, Xi He, Xinli Chen, Yujie Zhang, Qinjun Chen, Qin Guo, Tao Sun*, Chen Jiang

Key Laboratory of Smart Drug Delivery, Ministry of Education, State Key Laboratory of Medical Neurobiology, Department of Pharmaceutics, School of Pharmacy, Fudan University, Shanghai 200032, China

Received 3 July 2017; received in revised form 28 August 2017; accepted 27 September 2017

KEY WORDS

Human serum albumin;
Paclitaxel;
Drug delivery;
Substance P;
Blood–brain barrier;
Glioma

Abstract The blood–brain barrier (BBB) and the poor ability of many drugs to cross that barrier greatly limits the efficacy of chemotherapies for glioblastoma multiforme (GBM). The present study exploits albumin as drug delivery vehicle to promote the chemotherapeutic efficacy of paclitaxel (PTX) by improving the stability and targeting efficiency of PTX/albumin nanoparticles (NPs). Here we characterize PTX-loaded human serum albumin (HSA) NPs stabilized with intramolecular disulfide bonds and modified with substance P (SP) peptide as the targeting ligand. The fabricated SP-HSA-PTX NPs exhibited satisfactory drug-loading content (7.89%) and entrapment efficiency (85.7%) with a spherical structure (about 150 nm) and zeta potential of −12.0 mV. The *in vitro* drug release from SP-HSA-PTX NPs occurred in a redox-responsive manner. Due to the targeting effect of the SP peptide, cellular uptake of SP-HSA-PTX NPs into brain capillary endothelial cells (BCECs) and U87 cells was greatly improved. The low IC_{50}, prolonged survival period and the obvious pro-apoptotic effect shown by TUNEL analysis

Abbreviations: BBB, blood–brain barrier; BBTB, blood–brain tumor barrier; BCECs, brain capillary endothelial cells; Cou-6, coumarin-6; D_2O, deuterium oxide; DDS, drug delivery system; DHO, deuterium hydrogen oxide; DLS, dynamic light scattering; EE, entrapment efficiency; FACS, fluorescence-activated cell sorting; GBM, glioblastoma multiforme; gp60, glycoprotein 60; GSH, glutathione; HPLC, high performance liquid chromatography; HSA, human serum albumin; MAL-PEG-NHS, maleimide-polyethylene glycol-ω-succinimidyl carbonate; MTT, [4, 5-dimethylthiazol-2-yl]-2,5-diphenyl tetrazolium bromide; NK-1, neurokinin-1; NPs, nanoparticles; PBS, phosphate-buffered saline; PhAsO, phenylarine oxide; PI, propidium iodide; PTX, paclitaxel; SP, substance P; SPARC, secreted protein acidic and rich in cysteine; TEM, transmission electron microscope

*Corresponding author. Tel.: +86 21 51980187.
E-mail address: sunt@fudan.edu.cn (Tao Sun).

Peer review under responsibility of Institute of Materia Medica, Chinese Academy of Medical Sciences and Chinese Pharmaceutical Association.

http://dx.doi.org/10.1016/j.apsb.2017.09.008

all demonstrated that the fabricated SP-HSA-PTX NPs showed a satisfactory anti-tumor effect and could serve as a novel strategy for GBM treatment.

1. Introduction

Glioblastoma multiforme (GBM) is a kind of aggressive malignant brain cancer with the hallmark characteristics of uncontrolled cell proliferation and diffuse infiltration as well as the fatal prognosis with the median survival of less than 2 years[1,2]. Surgical methods still play the dominant role among the multiple approaches of GBM therapy, in which the bulk of the tumor is removed, but disappointingly, some peripheral parts are difficult to eradicate, leading often to relapse and metastasis[3]. Thus chemotherapy, a kind of noninvasive auxiliary treatment, remains indispensable for GBM patients. However, the blood–brain barrier (BBB) and blood–brain tumor barrier (BBTB) always serve as a formidable barrier to GBM treatments and severely limit the access of therapeutic agents to tumor cells within the brain[4]. Furthermore, the poor solubility, nonspecific distribution, rapid clearance and systemic toxicity of most chemotherapeutic drugs dramatically limits their applications, compromising the treatment efficiency and leading to severe adverse effects.

Recently, nanoparticulate drug delivery systems (DDS) have become a mature technical tool due to their optimized size and functionalized surface characteristics. The multifarious nanovehicles can package an existing drug to form various NPs which may improve the drug *in vivo* pharmacokinetic profiles, enhance drug accumulation at the targeted sites and thus further optimize therapeutic efficacy while avoiding toxic effects in healthy tissues[5]. However, the fact that the number of FDA approved products are much fewer than the preparations of the published achievements tells us that many challenges still remain in the optimization of the DDS from *in vitro* to *in vivo* translation, including lack of tolerability or high toxicity in patients as evidenced by the recall of many DDS formulations after commercialization[6]. Abraxane, one of the successfully marketed chemotherapy stars approved by the FDA in 2005 for the treatment of metastatic breast cancer, non-small cell lung cancer and pancreatic cancer[7] suggested to us that biomimetic materials originating from endogenous substances could be a favorable option with good biocompatibility and biodegradability. Thus, during the last decade we have witnessed an emerging paradigm shift to biomimetic materials due to their capacity to circumvent biological delivery barriers, along with increased specificity and compatibility with biological systems[8].

Among these biomimetics, albumin (also the vehicle used in Abraxane), an abundant and stable protein with a long circulatory half-life *in vivo*, has been explored as a versatile medical device for therapeutic and diagnostic agents due to its non-immunogenicity, inherent binding capacity for various drug molecules and targeting ability to malignant tissues by interacting with albumin-binding proteins, such as secreted protein acidic and rich in cysteine (SPARC) and glycoprotein 60 (gp60)[9–11]. Nevertheless, one of the obvious issues of an albumin-based drug delivery system is poor structural stability due to their native characteristics and the complex *in vivo* environment full of proteins and enzymes[12]. In terms of Abraxane, PTX molecules are not covalently linked to albumin, resulting in a poor stability in the circulation and unexpected PTX-leak before reaching the targets. Besides the tumor tissues, PTX is easily distributed into healthy organs, which will lead to wide systemic toxicity[13].

Inspired by the application of cross-linkers in polymeric micelles[14], we attempted to introduce a covalent linkage between the albumin molecules to improve physical adsorption between drugs and albumin. The abundant amino acids on albumin molecules contain 17 pairs of disulfide bonds that could be cleaved by reducing reagents. In an oxidative atmosphere intermolecular disulfide bonds can be reformed, leading to a re-assembly of the albumin molecules into relatively stable NPs and an improved encapsulating capability of drugs into the hydrophobic domain[15]. It is known that the level of glutathione (GSH), which can cleave disulfide bonds in tumor cells (10 mmol/L), is much higher than that in normal cells (0.2 mmol/L), which suggests that the intermolecular disulfide bonds between albumin molecules could be selected as an ideal self-cross-linker to realize preferred stabilization strategy of drugs as well as redox-responsive release in tumor cells[16,17].

Besides excellent *in vivo* stability and biocompatibility, efficient delivery of drugs is also necessary for a smart delivery system. The original uptake mechanism of albumin-based NPs is mainly mediated by SPARC and gp60 receptor. However, it is not enough to realize a favorable targeting effect in a complicated tumor microenvironment. Thus, some researchers have modified albumin NPs with various targeting moieties such as cetuximab[18], glycyrrhetinic acid[19] and cyclic Arg-Gly-Asp (RGD)[20] to achieve active targeting ability and promote drug accumulation in tumors. To endow the albumin NPs with passive targeting as well as active targeting ability to cross the BBB and BBTB effectively for the treatment of GBM, neurokinin-1 (NK-1) receptors are found to be selectively overexpressed in several malignant tumors including glioma[21]. SP peptide (with a sequence as Arg-Pro-Lys-Pro-Gln-Gln-Phe-Phe-Gly-Leu-Met) one of the NK-1 binding ligands, could be exploited as a targeting ligand on albumin NPs easily *via* a PEG linker.

In this study, we developed a glioma-targeting drug delivery system based on biomimetic albumin material with good stability and favorable biosafety. We first fabricated a stable human serum albumin (HSA) nanoparticle loaded with PTX (HSA-PTX NPs) with a redox-responsive characteristic and then SP peptide was covalently anchored on the HSA-PTX NPs (SP-HSA-PTX NPs) to improve tumor accumulation of PTX at the glioma site. The physicochemical properties of SP-HSA-PTX NPs, including particle size, surface morphology, drug loading and redox-responsive behaviors were studied in detail. Furthermore, the *in vitro* and *in vivo* therapeutic efficacy of the NPs was investigated in BCECs and U87 cells. Hopefully, this study will cast a new light for the biomimetic platform in tumor targeting delivery.

2. Materials and methods

2.1. Materials

HSA was purchased from Jiangxi Boya Biological Technology Co., Ltd. (Jiangxi, China). Thiol group-modified SP peptide was obtained from China Peptides Co., Ltd. (Suzhou, China). Maleimide-polyethylene glycol-ω-succinimidyl carbonate (MAL-PEG-NHS, MW: 3500) was purchased from Jenkem Technology (Beijing, China). The fluorescent probe BODIPY was synthesized as described previously. PTX, D-luciferin was purchased from Meilune Biological Technology Co., Ltd. (Dalian, China). Filipin, colchicines, phenylarine oxide (PhAsO) and (4, 5-dimethylthiazol-2-yl)-2,5-diphenyl tetrazolium bromide (MTT), propidium iodide (PI) and coumarin-6 (Cou-6) were purchased from Sigma–Aldrich (St. Louis, MO, USA). Other chemicals and all solvents were obtained from Sinopharm Group Co., Ltd. (Shanghai, China).

2.2. Cell lines and animals

The primary cultured BCECs were cordially provided by Prof. J.N. Lou (the Clinical Medicine Research Institute of the Chinese-Japanese Friendship Hospital, Beijing, China), which were cultured as described previously[22]. Human glioma cell line U87 MG was a gift from Prof. L.Y. Feng (Chinese Academy of Science, Shanghai, China). Glioma U87 cells expressing Photinuspyralis luciferase (U87-Luci) were gifts from Dr. N. Zhang (Caliper Life Sciences, A PerkinElmer Company, Shanghai, China). Both cell lines were cultured at 37 °C under a humidified atmosphere containing 5% CO_2.

Nude mice of 20–25 g body weight were purchased from the Department of Experimental Animals, Fudan University (Shanghai, China) and maintained under standard housing conditions. All animal experiments were carried out in accordance with guidelines approved by Fudan University' ethics committee.

2.3. Synthesis and preparation of HSA NPs

2.3.1. Synthesis of SP-HSA vectors

SP peptide-modified HSA (SP-HSA) was synthesized in two steps: First, NHS-$PEG_{3.5k}$-MAL was grafted to HSA as 10:1 ratio (mol/mol) in phosphate-buffered saline (PBS, pH 8.0) by stirring for 4 h at ambient temperature to form PEGylated HSA. The excess PEG was then removed by ultrafiltration using a 10 kDa molecular weight cutoff (MWCO) membrane. After that, the final vector SP-HSA was prepared by adding the SP peptide into the PEGylated HSA solution (5:1 ratio, mol/mol) allowing the reaction between the thiol groups of SP peptide and MAL groups of PEGylated HSA in PBS (pH 8.0) to proceed for 5 h at room temperature. NHS-PEG-OCH_3 was used to directly react with HSA *via* the same method to obtain the PEGylated HSA for the following HSA-PTX NP preparation.

2.3.2. Preparation of SP-HSA-PTX NPs and HSA-PTX NPs

SP-HSA-PTX NPs and HSA-PTX NPs were prepared by the reported method with minor modification[23,24]. SP-HSA or PEGylated HSA was first treated with 50 mmol/L GSH in deionized water for 4 h at 37 °C to cleave the inner intramolecular disulfide bonds to free sulfhydryl groups. Next, the solution was dialyzed (MWCO 3500) for 24 h under N_2 to remove the excess GSH, followed by a freeze-drying. Finally, 1 mL of ethanol contained 2 mg of PTX solution was added dropwise into 1 mL PBS (pH 7.4) contained 20 mg of SP-HSA or PEGylated HSA solution with appropriate stirring speed. The suspension was stirred at room temperature for another 30 min and then H_2O_2 (aqueous, 30%, 20 μL) was added to form intermolecular disulfide bonds again. Next, the ethanol was removed quickly using rotary evaporators. Finally, the suspension was purified by ultrafiltration (MWCO 10 kDa) to remove free PTX and ethanol. The preparation is shown in Scheme 1.

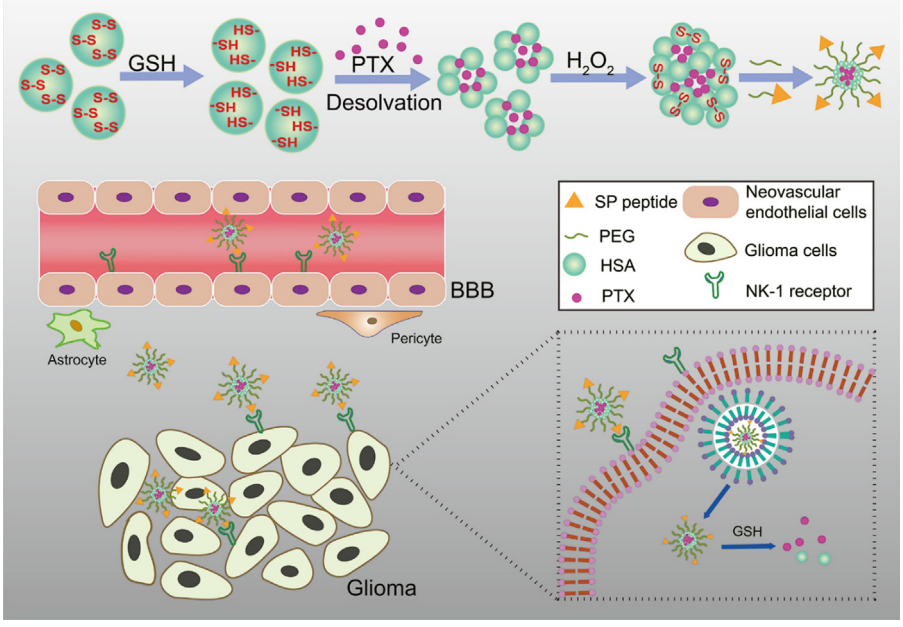

Scheme 1 The preparation of SP-HSA-PTX NPs and the dual targeting (BBB and glioma cells) process *in vivo*.

2.4. Physicochemical characteristics of HSA NPs

The final product SP-HSA was characterized by ^{1}H NMR spectra measured by NMR spectrometer (Bruker, Billerica, MA, USA) in deuterium oxide (D_2O) and deuterium hydrogen oxide (DHO) as internal reference. The average size and ζ potential of HSA NPs were measured by dynamic light scattering (DLS, Zetasizer Nano-ZS, Malvern, Worcestershire, UK). The morphology of SP-HSA-PTX NPs was characterized by transmission electron microscope (TEM, JEOL JEM-1200EX, Tokyo, Japan).

To determine the drug loading and entrapment efficiency (EE), HSA-PTX NPs and SP-HSA-PTX NPs were first treated with tyrisin 1:2 (*v*/*v*) at 37 °C for 2 h, and then diluted in 2 mL of methanol and sonicated for another 30 min to completely extract PTX according to the reported method[24]. The PTX amount was determined on a high performance liquid chromatography (HPLC) system, an Agilent 1260 series device (Palo Alto, CA, USA) equipped with an UV detector set at 227 nm and a reverse C18 column (250 mm × 4.6 mm, 5 μm). The adopted mobile phase consisted of acetonitrile and water (60:40, *v*/*v*) and the flow rate was maintained at 1.0 mL/min. The drug loading and EE were calculated as previously described[25].

2.5. In vitro redox-responsive behaviors of HSA NPs

First, Ellman's test was used to determine the transition from intermolecular to intramolecular disulfide bonds by detecting the sulfhydryl content (see Supporting Information). The PTX release behavior of HSA NPs was measured by a dialysis method ($n = 3$). In brief, a 0.3 mL solution of HSA NPs (0.5 mg/mL PTX) was sealed into a dialysis bag (MWCO 3500). Then the bag was immersed into 12 mL of PBS buffer (pH 7.4) containing 0.1% (*v*/*v*) Tween 80 with or without 10 mmol/L GSH to maintain the silk condition and shaken at 100 rpm at 37 °C. An aliquot of release solution (0.2 mL) at each predetermined time point was withdrawn for HPLC assay and the same volume of fresh medium was replenished.

2.6. In vitro cytotoxicity assay

The cytotoxicity of each formulation to U87 cells was assessed by MTT assay ($n = 6$). U87 cells were seeded in 96-well plates at a density of 5×10^3 cells per well and incubated at 37 °C for another 24 h. When 80% confluence was achieved the cells were treated with fresh media containing free PTX and different HSA-PTX formulations at various concentrations of PTX (0.001 to 20 μg/mL), and then the cells were cultured for 24 h at 37 °C after which the medium was removed. A control group was set up to represent cells without any treatment. MTT solution (100 μL, 5 mg/mL) was added to each well and incubated for an additional 4 h. The supernatants were replaced by 150 μL of DMSO per well and shaken for 10 min at 37 °C. Absorbance was measured at 570 nm using a microplate reader.

2.7. Cellular uptake and internalization mechanism assay

A fluorescent inverted microscope (DMI4000 B, LEICA, Wetzlar, Germany) was used to visualize the cellular uptake efficiency of HSA NPs, using Cou-6 as the fluorescent probe. As for the preparation of HSA-Cou-6 NPs and SP-HSA-Cou6 NPs, similar to the PTX incorporation, a solution of 0.5 mg Cou-6 dissolved in 2 mL of ethanol was dripped into SP-HSA or HSA solution to form different Cou-6 formulations. The BCECs and U87 cells were seeded in 24-well culture plates at a density of 5×10^4 cells per well and incubated at 37 °C for 24 h. When 80% confluence was achieved, both cells were incubated with 200 μg/mL HSA/Cou-6 NPs and SP-HSA/Cou6 NPs for 0.5 h. After the incubation, cells were washed three times with D-Hank's solution and photographed by fluorescence microscopy.

Quantitative analysis of cellular uptake of HSA NPs was assessed by fluorescence-activated cell sorting (FACS, BD Biosciences, Bedford, MA, USA). The BCECs and U87 cells were seeded in 6 well plates at a density of 4×10^4 cells per well and incubated at 37 °C for 24 h. After 80% confluence was reached, the medium was replaced with different HSA NPs described above and incubated for 0.5 h. After the incubation, cells were washed three times with D-Hank's solution and collected after digestion, subjected to centrifugation at 1500 rpm (TG16-WS, Cence, Hunan, China) for 5 min and analyzed using a flow cytometer. For each sample, 10,000 events were collected and analyzed. Cells cultured under normal conditions served as control.

To investigate the mechanism of internalization, the BCECs and U87 cells were first preincubated with different inhibitors at 37 °C for 15 min, including 10 μmol/L free SP peptide, 1 μg/mL filipin, 1 μg/mL colchicine, and 0.3 μg/mL PhAsO as different kinds of endocytic inhibitors. Then, 200 μg/mL SP-HSA-Cou6 NPs was added to each well. After incubation for 30 min, the medium were discarded and the cells washed three times with D-Hank's solution. Both qualitative and quantitative analyses were performed as described above.

2.8. Cell-cycle assay

U87 cells were seeded in 6 well plates at a density of 4×10^5 cells per well and incubated at 37 °C for 24 h. After 80% confluence was reached, cells in each well were replaced with fresh media containing free PTX, HSA-PTX NPs, and SP-HSA-PTX NPs (equivalent to 5 μg/mL of PTX) at 37 °C for 12 h. Next, the cells were further cultured at 37 °C for 12 h and then washed with PBS and fixed with 500 μL of cold ethanol (70%) for 2 h. Cells were further washed with PBS and treated with RNase A for 30 min and then with 200 μL of propidium iodide (PI) for 30 min at 4 °C. The stained cells in each sample were detected with a FACS Calibur flow cytometer, and the percentage of cell cycle phases and apoptosis was analyzed using Flowjo 6.0.

2.9. Animal model establishment

All animal experiments were carried out in accordance with guidelines evaluated and approved by the ethics committee of Fudan University, Shanghai, China. To establish the glioma model, nude mice were anaesthetized by chloral hydrate (10%) and slowly injected with U87-Luci cells (1×10^5 cells/5 μL) at striatum, 1.8 mm right lateral to the bregma and 3 mm of depth.

2.10. In vivo biodistribution of SP-HSA-BODIPY NPs and HSA-BODIPY NPs

To visualize the *in vivo* real-time distribution, tetraaryl analogue 1 (BODIPY), which has an excitation λ_{max} at 700 nm and emission at 729 nm was selected as the fluorescent probe *in vivo* and was encapsulated into HSA NPs, referring to the same preparation method described above. In brief, 1 mL ethanol contained 0.1 mg of BODIPY

solution was quickly dripped into 20 mg GSH-treated SP-HSA or PEGylated HSA solution with appropriate stirring speed. The suspension was stirred at room temperature for another 30 min and then H_2O_2 (aqueous, 30%, 20 μL) was added to form the different NPs. Finally, ethanol was removed by rotary evaporators. On the 14th day after glioma implantation, tumor-bearing nude mice were intravenously injected with HSA-BODIPY NPs and SP-HSA-BODIPY NPs at a BODIPY dose of 0.5 mg/kg. Then at 1, 2, 8, and 12 and 24 h after administration, the mice were anesthetized and visualized under IVIS Spectrum *in vivo* image system (Caliper, Newton, MA, USA). After that, mice were sacrificed and the glioma-bearing brains and other main organs (heart, liver, spleen, lung, and kidney) were excised for further visualization by IVIS.

2.11. *In vivo antitumor efficacy assay*

Glioma-bearing mice were randomly divided into four groups ($n = 7$) and treated with HSA-PTX NPs, SP-HSA-PTX NPs, Taxol at a dose of 10 mg/kg PTX and saline at days 15, 18 and 21, respectively (the implantation day was day 0). The body weight of each animal was measured every 2 days. At different days during the treatment, mice were injected intraperitoneally with D-luciferin (3 mg per mouse) to evaluate the signal of tumor. The efficacy of different formulations was further evaluated by measuring the body weight and survival term of the animals after the treatments. The TUNEL assay was used to further validate the apoptotic efficacy. After treatment with different NPs, the mice were killed and brains were removed for frozen sectioning. The sections were treated according to the instructions of the kit to detect the broken nuclear DNA fragments, stained with DAPI, and observed under the fluorescent microscope.

2.12. *Statistical analysis*

All data are represented as means ± SD. Analysis was performed with GraphPad Prism software.

3. Results

3.1. *Preparation and characterization of HSA NPs*

PEG-HSA was first synthesized successfully by linking the NHS group on NHS-PEG-MAL to the amino group on HSA. Thiol group-modified SP peptide was then conjugated *via* the reaction between the MAL group and a thiol group on HSA to fabricate the targeting moiety. In the ^{1}H NMR spectrum shown in Fig. 1, the multiple characteristic peaks of SP were found in SP-HSA molecules, suggesting a successful conjugation. HSA-PTX NPs were prepared by a desolvation method. The mean size of SP-HSA-PTX NPs is slightly higher than HSA-PTX NPs due to the conjugation with SP peptide. The TEM results further defined the morphology of SP-HSA-PTX NPs (Fig. 2). The physicochemical characteristics and loading parameters are shown in Table 1. The ζ potential of HSA-PTX NPs and SP-HSA-PTX NPs was about −13.5 and −12.8 mV, respectively. The drug-loading content of both formulations was around 10%, with nearly 90% showing satisfactory entrapment efficiencies.

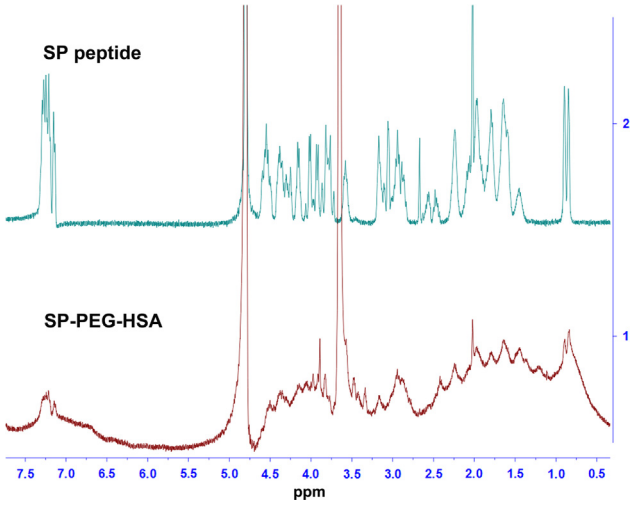

Figure 1 Corresponding ^{1}H NMR spectra of SP peptide and SP-PEG-HSA.

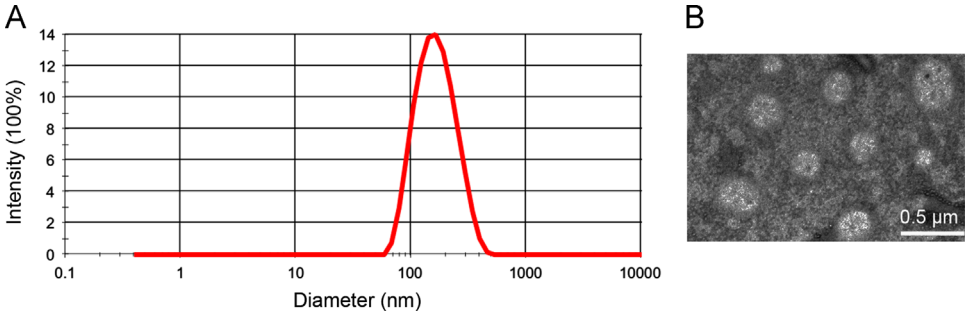

Figure 2 Size distribution (A) and TEM image of SP-HSA-PTX NPs (B).

Table 1 Physical characterization of HSA-PTX NPs and SP-HSA-PTX NPs.

Nanoparticle	HSA-PTX NP	SP-HSA-PTX NP
Size (nm)	154.2 ± 12.6	168.2 ± 10.3
PDI	0.204 ± 0.047	0.195 ± 0.031
Zeta potential (mV)	−13.5 ± 6.8	−12.8 ± 3.5
Drug loading (%)	8.31 ± 3.15	7.89 ± 1.31
EE (%)	87.5 ± 1.3	85.7 ± 2.6

Data are represented as mean ± SD ($n = 3$).

3.2. *In vitro redox-responsive behaviors of HSA NPs*

To study the stability and redox-responsiveness of the intermolecular disulfide bonds on PTX leakage from HSA NPs, we investigated the PTX release behaviors in PBS buffer (pH 7.4) with or without 10 mmol/L GSH, mimicking the concentration in tumor cells. As shown in Fig. 3, free PTX underwent an initial burst release in which nearly 80% PTX was released within 4 h, while the release rate of SP-HSA-PTX NPs was much slower and less than 40% PTX was detected up to 48 h. However, when exposed to the medium of intracellular GSH concentration (~10 mmol/L), PTX release was greatly boosted with more than 40% of the PTX released within 2 h and approximate 75% after 48 h.

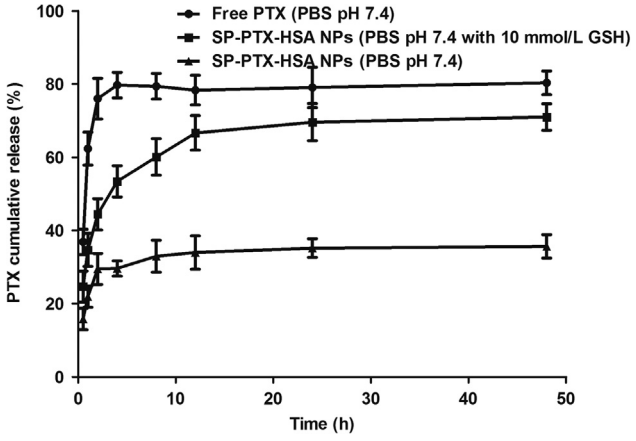

Figure 3 *In vitro* drug release profiles of SP-HSA-PTX NPs in different mediums with free PTX as the control group. Data are represented as mean ± SD ($n = 3$).

3.3. *In vitro cytotoxicity assay*

The *in vitro* cytotoxicity of free PTX and different PTX loaded-HSA NPs against U87 cells was assessed by an MTT assay. Fig. 4 revealed that different PTX formulations have various inhibitory effects in a dose-dependent manner on U87 cells. It was found that the IC_{50} values of SP-HSA-PTX NPs and HSA-PTX NPs were significantly lower than that of free PTX, indicating that the encapsulation of PTX in HSA NPs and the redox-responsive release behavior facilitated the PTX internalization and intracellular release in cells. Besides that, owing to the targeted binding of SP peptide to U87 cells, the SP-HSA-PTX NPs (IC_{50} = 121.1 ng/mL) showed much more toxicity than HSA-PTX NPs (IC_{50} = 294.8 ng/mL, Supplementary Information Table S2).

3.4. *Cellular uptake and internalization mechanism assay*

We evaluated the cellular uptake characteristics and the possible mechanisms of HSA NPs on BCECs and U87 cells using Cou-6 as the fluorescent probe (Fig. 5A). Graphics captured by fluorescence microscopy indicated that the cellular uptake of SP-HSA-Cou-6 NPs on both cell lines was significantly higher than that of HSA-Cou-6 NPs, indicating the dual targeting effect of the SP peptide, namely that the SP peptide could act with the NK-1 receptors on both vascular endothelial cells and tumor cells, resulting in higher cellular uptake of NPs. Meanwhile, the level of internalization of SP-HSA-Cou-6 NPs was

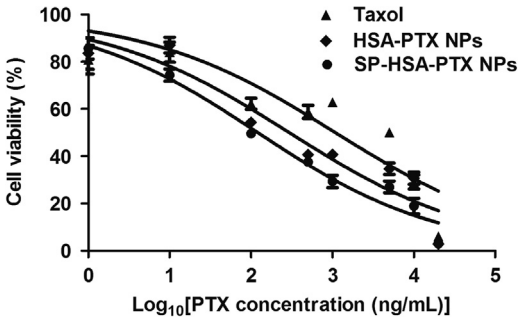

Figure 4 *In vitro* cytotoxicity of different PTX formulations at various concentrations against U87 cells. Data are represented as mean ± SD ($n = 6$).

concentration-dependent. Consistent with the qualitative analysis, quantitative analysis with flow cytometry exhibited the corresponding internalization manner in which the fluorescent intensities of SP-HSA-Cou-6 NPs were higher than HSA-Cou-6 NPs (Fig. 6A).

To further investigate the possible internalization mechanism of SP-HSA-Cou-6 NPs, the endocytosis pathways were inhibited by various inhibitors, including free SP peptide, PhAsO, filipin and colchicine. Fig. 5B shows that the internalization of SP-HSA-Cou-6 NPs was inhibited remarkably both on BCECs and U87 cells after treatment with free SP peptide. Additionally, different endocytic inhibitors further confirmed the receptor-mediated endocytosis pathway. Among the three endocytic inhibitors, PhAsO exhibited the most significant inhibitory effect, indicating that the main endocytosis pathway of SP-HSA-Cou-6 NPs was clathrin-mediated endocytosis. Consistent with the qualitative analysis, the quantitative analysis also showed similar results (Fig. 6B).

3.5. *Cell cycle assay*

Given that PTX's mode of action is disruption of microtubule dynamics and the formation of microtubule is specific in the G2 phase of cell cycle, we quantified the population of U87 cells in different stages of the cell cycle upon treatment with different PTX formulations to evaluate the potential inhibitory effect on G2 phase and cell proliferation. As shown in Fig. 7, SP-HSA-PTX NPs exhibited the highest cell percentage in the G2 phase (49.74%) compared with HSA-PTX NPs (42.12%) and free PTX (39.81%), suggesting the distinct inhibitory effect on cell proliferation.

3.6. *In vivo biodistribution of SP-HSA-BODIPY NPs*

To further evaluate the glioma-targeting effect, different BODIPY loading HSA NPs were intravenously injected into U87-Luci tumor-bearing nude mice and observed under an *in vivo* image system. As displayed in Fig. 8A, mice treated with SP-HSA-BODIPY NPs exhibited a stronger fluorescent signal in the tumor area 24 h after injection compared with the HSA-BODIPY NPs, which was mainly due to the specific binding of SP peptide to the BBB and brain tumors. After that, glioma-bearing brains and major organs were excised for *ex vivo* imaging to reveal the tissue distribution of HSA NPs. As

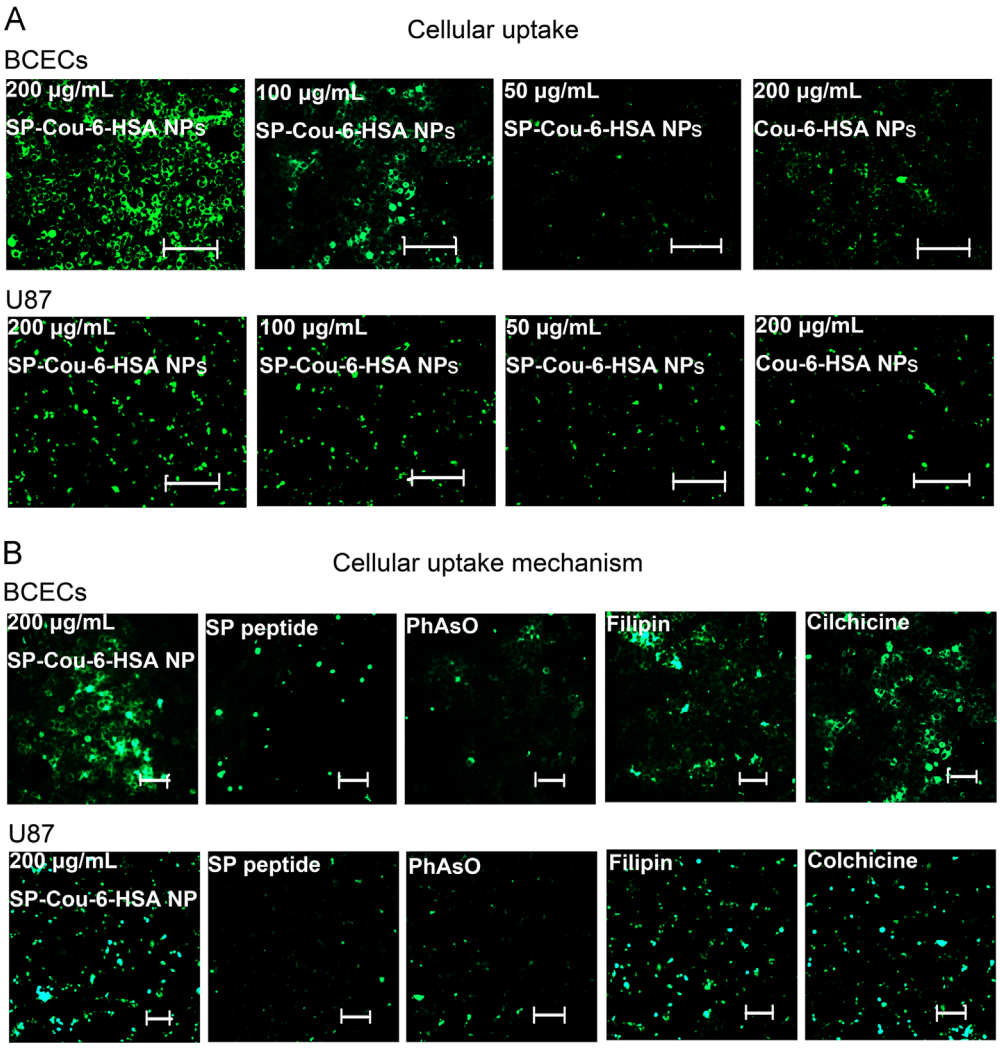

Figure 5 Cellular uptake of HSA-Cou-6 NPs and SP-HSA-Cou-6 NPs with different concentrations in BCECs and U87 cells 30 min after incubation (A) (scale bar: 80 μm). Possible uptake mechanism of SP-HSA-Cou-6 NP internalization into BCECs and U87 cells. The cells were blocked by different inhibitors (B) (scale bar: 40 μm).

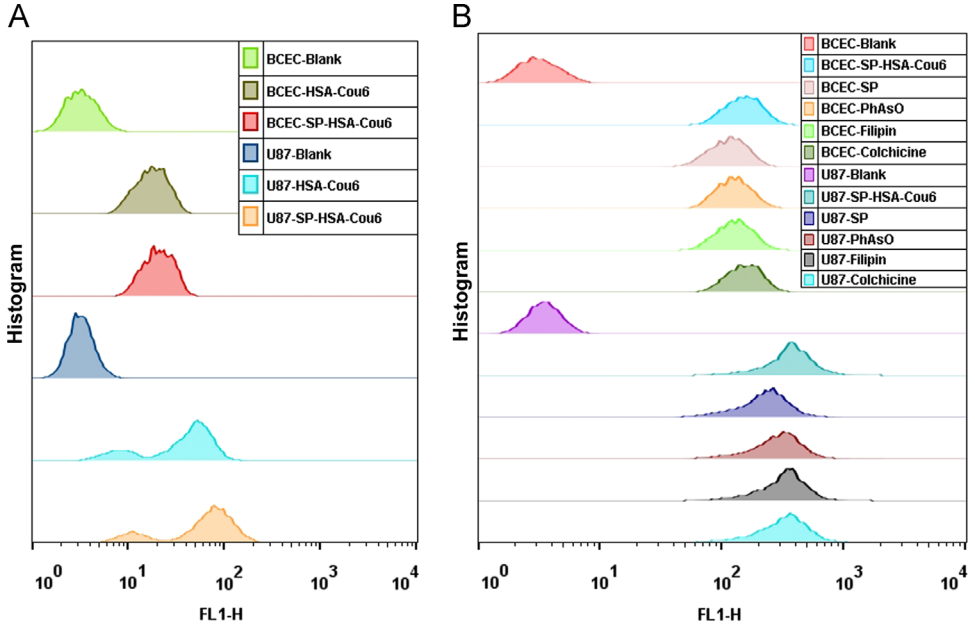

Figure 6 Flow cytometric quantitative analysis of cellular uptake (A) and the uptake mechanism experiment (B).

indicated in Fig. 8C, the SP peptide targeting group exhibited less fluorescent signal in the liver compared with non-targeting group, suggesting lower toxicity to the liver. The distribution of NPs in the heart, spleen, lung, and kidney was similar in both two groups.

3.7. *In vivo antitumor efficacy assay*

The *in vivo* antitumor effects of different formulations were evaluated on the glioma model mice bearing with U87-Luci cells (Figs. 9 and 10). Luciferase expression in the tumor site was visualized with the injection of luciferin and imaged by IVIS and the luminescence intensity represented the tumor progression in the brain (Fig. 9A). The images of bioluminescence intensity of mice treated with SP-HSA-PTX NPs nearly remained the same while the other groups exhibited increasing intensity, suggesting the strongest anti-tumor efficacy of SP-HSA-PTX NPs. Semi-quantitative luminescence intensity variation indicated the growth of the tumor (Fig. 9B). From the collected data from four groups, the luminescence intensity in SP-HSA-PTX NP group was weaker than other three groups, exhibiting the most remarkable antitumor efficacy. Moreover, there was a significant difference between SP-HSA-PTX NP and free PTX groups. Besides, luminescence intensity in the saline group sharply increased during the treatment duration. After completion of the treatment, the whole brain was dissected to evaluate the tumor apoptosis among different groups using TUNEL assay. As shown in Fig. 11, there was nearly no apoptotic signal in the saline group and Taxol group. The apoptotic cases in HSA-PTX NPs were better than the above-mentioned groups, while the SP-HSA-PTX NPs group displayed the most remarkable apoptotic phenomenon. Additionally, as expected, the SP-HSA-PTX NP group exhibited the longest survival time and achieved the greatest antitumor efficacy (Fig. 10).

4. Discussion

Currently, chemotherapy is still the indispensable therapeutic regimen for patients diagnosed with GBM, a highly aggressive tumor. However, due to the BBB and the inherent defects of most therapeutic agents, such as water insolubility, premature degradation and non-specific distribution, the therapeutic effects of many drugs are greatly weakened. The emerging DDS strategy and the great success on multiple tumor patients of Abraxane cast a new light on the construction of drug carriers with biomimetic materials such as apoferritin[26] and liquid membrane[27]. However, the drug binding capacity mainly depends on the physical absorption or packet loading of the materials, leading to poor plasma stability[28]. In this study, in view of the pathological

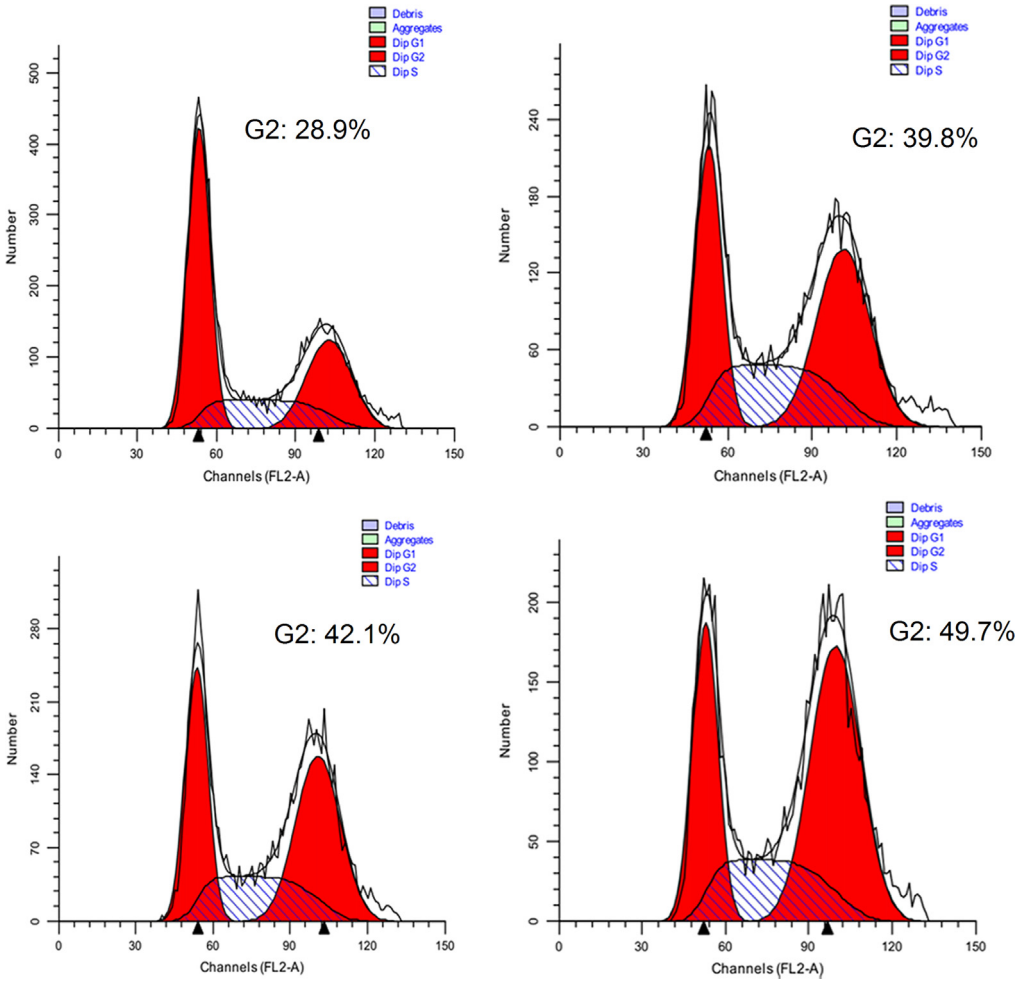

Figure 7 Representative cell cycle distribution of U87 cells after incubation with Taxol (B), HSA-PTX NPs (C), and SP-HSA-PTX NPs (D) at the equivalent drug concentration by flow cytometry and the negative control group (A).

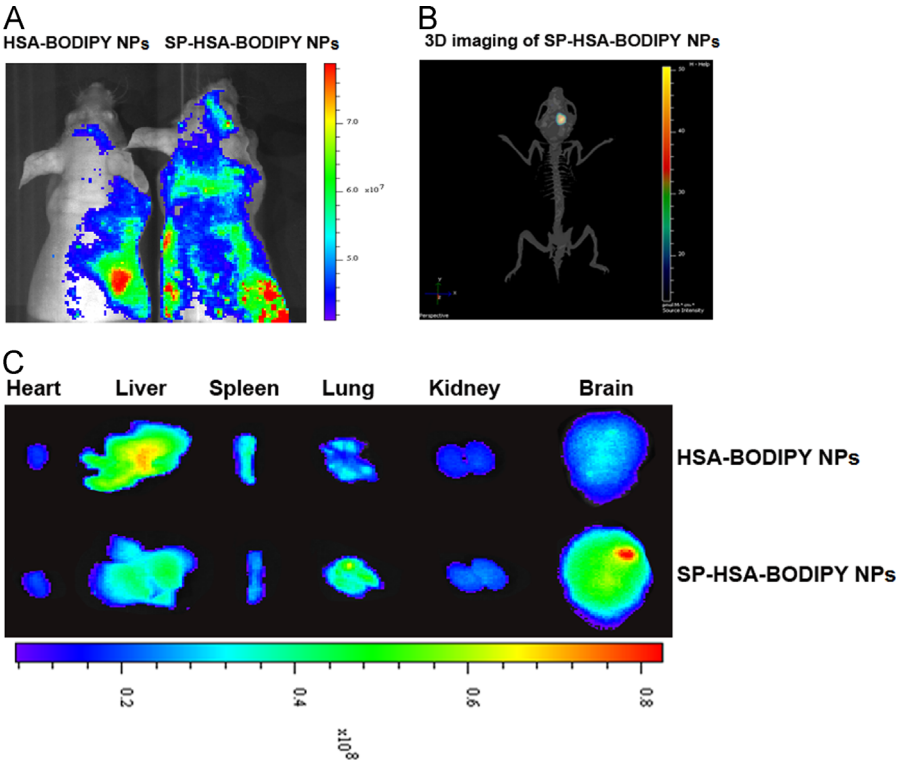

Figure 8 *In vivo* and *ex vivo* distribution of HSA-BODIPY NPs and SP-HSA-BODIPY NPs after intravenous administration. Images were taken 24 h after injection (A) and 3D imaging 24 h after i.v. injection of SP-HSA-BODIPY NPs (B). Representative *ex vivo* images of brains and organs of mice sacrificed at 24 h.

features of GBM and defectiveness of bioinspired nanocarriers, a self-cross-link strategy was introduced to fabricate a stable albumin-based drug delivery system that was modified with a targeting group, thus creating greater efficacy to GBM treatment. SP, as a neuropeptide released from the endings of sensory nerve fibers, can specifically bind with NK-1 receptor which is widespread throughout CNS tumors such as glioma[29]. Herein, SP peptide was employed as the targeting group to achieve the dual BBB-crossing and glioma-targeting ability.

SP peptide-modified HSA molecules were facilely synthesized through a classic reaction between a MAL and a thiol group. The PTX-loaded HSA NPs were prepared by a desolvation method and stabilized by intramolecular disulfide bonds. In the preparation process the amount of sulfhydryl group was measured by the Ellman's method. As indicated in Supplementary Information Table S1, the number of free thiol group increased from 0.43 to 4.10 after GSH reduction, and further decreased back to 0.51 upon the formation of HSA-PTX NPs, demonstrating the transition from intermolecular into intramolecular disulfide bonds. In the process of albumin NP formation, it was noteworthy that the ratio of ethanol/PBS, the amount of PTX/albumin, the temperature and stirring rate should be strictly and carefully tailored to prevent precipitation. Considering that excessive modification with a targeting moiety to PEG could result in a fast removal by the immune system *in vivo*, the optimized modification degree of SP peptide was about 50%[16]. The physicochemical characterization results revealed that the resultant SP-HSA-PTX NPs exhibited a spheroidal structure of about 150 nm, satisfactory drug-loading content and entrapment efficiencies (Table 1). The mean size of SP-HSA-PTX NPs measured by DLS was 168.2 ± 10.3 nm diameter, which is slightly larger than the TEM result given that the DLS analysis reflects the hydrated state of NPs while the TEM was obtained under the solid state with fewer aggregation and better dispersity.

The drug release kinetics study is crucial in evaluating different formulations. The drug release behavior was monitored to verify the stable and redox-responsive characteristic of SP-HSA-PTX NPs. Fig. 3 showed that few PTX molecules were released from the NPs in PBS buffer ascribing to the stabilizing effect of intermolecular disulfide bonds, while the release rate was remarkably enhanced when exposed to the intracellular GSH level (10 mmol/L GSH), suggesting redox-responsive behavior. Besides that, the IC_{50} of SP-HSA-PTX NPs and HSA-PTX NPs were significantly lower than Taxol, which also proved the higher intracellular PTX release and the redox-responsive behavior in cells (Fig. 4). These findings suggested that the disulfide bond-cross-linked SP-HSA-PTX NPs could maintain integrity and stability in the extracellular environment, which had an advantage over the marketed Abraxane in virtue of being able to prevent drug leakage before reaching the tumor lesion and reducing toxicity to normal tissues. However, drug release was immediately activated with the aid of abundant GSH in tumor cells, which contributed to rapid and efficient drug accumulation to make a favorable therapeutic effect in time.

Next, the *in vitro* anti-tumor effect was investigated on BCECs and U87 cells. BCECs play a major role in constructing BBB and in this study we selected BCECs to evaluate the BBB permeability of different NP[30]. Based on the qualitative and quantitative assays, the cellular uptake of SP-HSA-Cou-6 NPs on BCECs and U87 cells were both significantly higher than the HSA-Cou-6 NPs at the same concentration, indicating that the NK-1 receptors that can recognize SP peptide were overexpressed both on the BCECs and

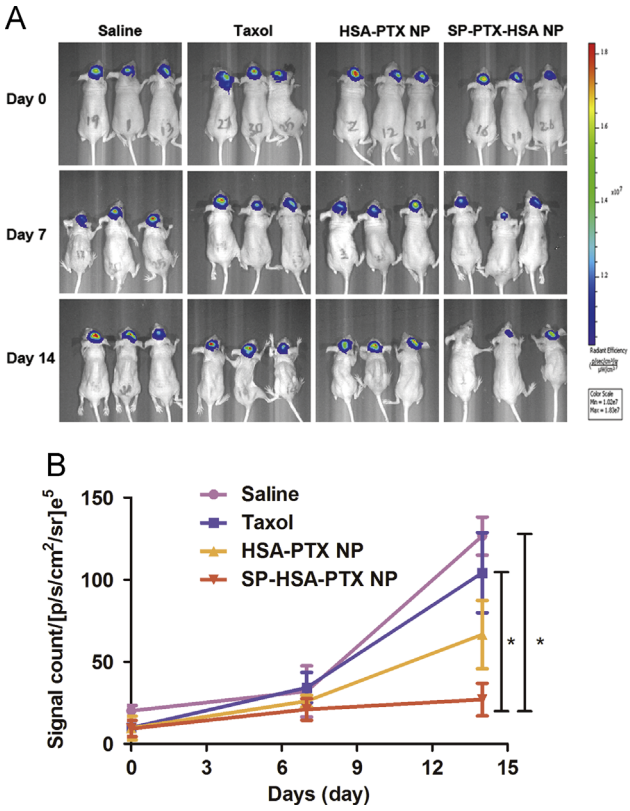

Figure 9 Anti-glioma efficacy of different PTX formulations on model mice. Real-time bioluminescence images of the glioma model nude mice injected with saline, Taxol, HSA-PTX NPs and SP-HSA-PTX NPs on days 0, 7 and 14 (A). Semi-quantification results of signals of each mouse (B). Data are represented as mean ± SD ($n = 3$), $^{*}P < 0.05$.

U87 tumor cells, causing dual-targeting capacity of the SP peptide to permeate the BBB and bind to the glioma cells. The downside of this study was, of course, it was better to choose the transwell assay to simulate the *in vitro* BBB model and evaluate the penetration effect[31,32]. The excessive free SP peptide treatment could greatly inhibit the internalization of SP-HSA-Cou-6 NPs due to competitive inhibition and the receptor-saturation effect, which further showed that the SP peptide was responsible for the targeting ability to increase the cellular uptake (Figs. 5 and 6). In addition, the MTT results demonstrated that the SP-HSA-PTX NPs gave rise to the strongest anti-tumor effects resulting from the synergistic role of the enhanced cellular uptake and redox-responsive behavior in cells (Fig. 4). Besides satisfactory cellular uptake, the drug is also expected to be effectively released from the carrier. Apparently, the SP peptide endowed the SP-HSA-PTX NPs with enhanced accumulation into cells, then the high GSH concentration in the cytoplasm triggered the cleavage of disulfide bonds, and the NP disassembled along with release of encapsulated PTX, which finally generated sufficient drug concentration in tumor cells. The anti-tumor mechanism of PTX depends on mitotic delay through microtubule stabilization and eventually arrests cell cycle in G2 phase.[33] As expected, the proportion of cells in G2 phase was increased when exposed to different PTX formulations compared with the control group. Additionally, SP-HSA-PTX NPs showed the highest G2 fraction and were in line with the MTT results. As mentioned above, the cell experiments showed the advantage of the self-cross-link and SP modification strategy in

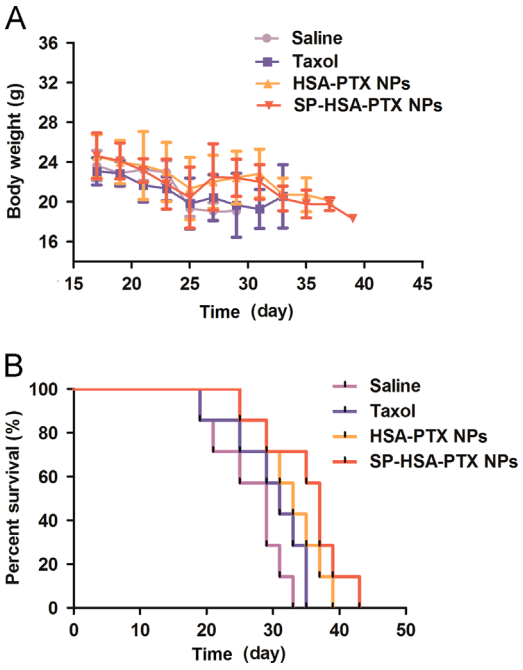

Figure 10 Overall survival curves (A) and body weight change (B) of mice treated with different formulations ($n = 7$).

encapsulating PTX into nanovehicles and preliminarily demonstrated the *in vitro* efficient tumor targeted therapy of SP-HSA-PTX NPs.

Encouraged by the exciting *in vitro* results, we further conducted a series of *in vivo* therapy evaluations. First, the targeting capacity of SP peptide to BBB and tumor cells as well as the tissue distribution of HSA NPs were visualized under the IVIS system through tail intravenous injection to the glioma-bearing nude mice. Based on the enhanced permeability and retention (EPR) effect, the GP60, SPARC and NK-1 receptor-mediated targeted pathway, the BODIPY signal of mice treated with SP-HSA-BODIPY NPs was sustained until 24 h and was stronger than the non-targeted group (Fig. 8A), which also manifested the encouraging long stability in the blood circulation. The *ex vivo* images also confirmed the brain-tumor-targeting ability of SP-HSA-BODIPY NPs (Fig. 8C). It should be noted that the fluorescence signal obtained from SP-HSA-BODIPY NPs in liver, one of the vital organs of metabolism, was lower than HSA-BODIPY NP group, which showed that the fabricated nanoparticle could decrease elimination and alleviate the burden of liver. Finally, the anti-tumor effect was evaluated through the luminescence intensity variation and the survival time difference. As shown in Fig. 9, as the control, the saline group showed fast proliferation of tumor cells. Tumor growth in the free PTX and HSA-PTX NP groups were relatively slower, and as expected, the SP-HSA-PTX NP group exhibited the most remarkable anti-tumor effect, where the curve was nearly flat. Fig. 10 shows that the SP-HSA-PTX NP group possessed the longest median survival time compared with other groups. In summary, taken together the results of the lowest luminescence intensity in tumor foci, the strongest apoptotic signal, the longest survival time and the slowest body weight loss (Figs. 9–11), indicated that SP-HSA-PTX NPs exhibited the best therapeutic efficacy compared with HSA-PTX NPs and Taxol, which may be attributed to the sufficient PTX accumulation at tumor site and reduced systemic adverse effects. The HSA-PTX NP group did possess a prolonged survival time, which could be attributed to the enhanced accumulation by EPR effect and the

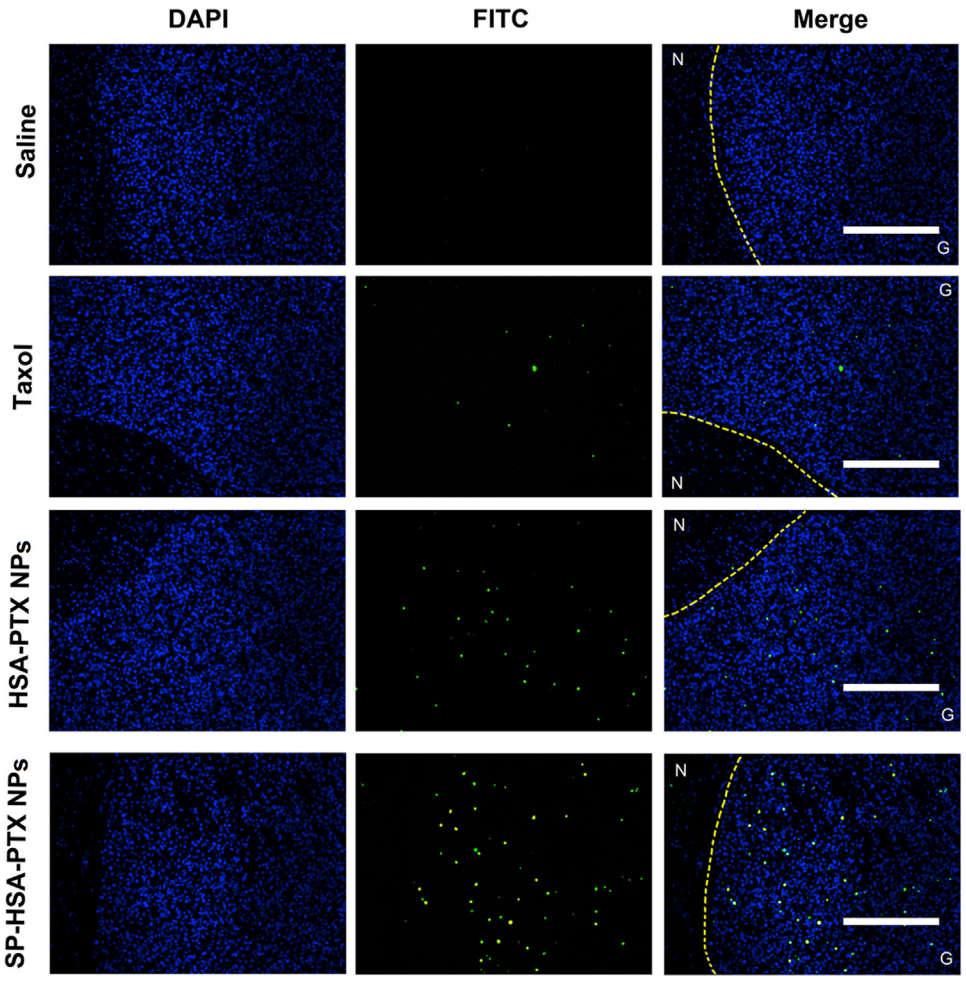

Figure 11 TUNEL assay of frozen sections of brain tumors after treatment with different formulations. Green: TUNEL-stained apoptosis cells. Blue: DAPI-labeled nucleus. Dashed line: boundary between normal brain section and glioma section. N: normal brain section. G: glioma section. (Original magnification: 100 × , scale bar: 100 μm).

original targeting ability of albumin, which provided nutrition and energy to the fast growth of tumor[34,35]. The *in vivo* results are in accordance with the *in vitro* results. Besides an efficient therapeutic effect, safety is another indispensable factor for an ideal drug delivery system. Finally, we observed the histological status of the heart, liver, spleen, lungs, and kidneys through H&E staining, which indicated that there were no obvious toxic pathological changes in the SP-HSA-PTX NP group (Supplementary Information Fig. S1).

Taking all the results into account, this study convincingly shows the satisfactory anti-tumor effect of SP-HSA-PTX NPs and puts forward a novel strategy for GBM treatment with efficient therapy and favorable biosafety.

5. Conclusions

In summary, we developed a stable SP-modified intramolecular disulfide bond cross-linked albumin nanoparticle as a satisfactory drug delivery vehicle for the treatment of GBM. This drug delivery system exhibited the following features: (i) favorable biocompatibility; (ii) improved stability and minimal drug leakage during circulation *in vivo* due to the existence of intramolecular disulfide bonds; (iii) specific tumor targeting ability through the EPR effect and SP-mediated binding to BBB and tumor cells; (iv) intracellular drug release under the high GSH concentration. The results indicate that the SP-HSA-PTX NPs exhibited good stability, enhanced the drug accumulation in tumor sites and induced stronger anti-tumor effect, meanwhile with low systemic toxicity. The work may provide a novel platform for the application of biomimetic materials in the tumor therapy.

Acknowledgments

This work was supported by the National Natural Science Funds of China (21602030 and 81172993), National Basic Research Program of China (973 Program, 2013CB932500), Shanghai Sailing Program (16YF1400900), Scientific Research Foundation of Fudan University for Talent Introduction (JJF301103), National Science Fund for Distinguished Young Scholars (81425023).

Appendix A. Supporting information

Supplementary data associated with this article can be found in the online version at http://dx.doi.org/10.1016/j.apsb.2017.09.008.

References

1. Hu Q, Gao X, Gu G, Kang T, Tu Y, Liu Z, et al. Glioma therapy using tumor homing and penetrating peptide-functionalized PEG–PLA nanoparticles loaded with paclitaxel. *Biomaterials* 2013;**34**:5640–50.
2.. Anjum K, Shagufta BI, Abbas SQ, Patel S, Khan I, Shah SA, et al. Current status and future therapeutic perspectives of glioblastoma multiforme (GBM) therapy: a review. *Biomed Pharmacother* 2017;**92**:681–9.
3. Newton HB. Advances in strategies to improve drug delivery to brain tumors. *Expert Rev Neurother* 2006;**6**:1495–509.
4. Biddlestone-Thorpe L, Marchi N, Guo K, Ghosh C, Janigro D, Valerie K, et al. Nanomaterial-mediated CNS delivery of diagnostic and therapeutic agents. *Adv Drug Deliv Rev* 2012;**64**:605–13.
5. Zhang Y, Chan HF, Leong KW. Advanced materials and processing for drug delivery: the past and the future. *Adv Drug Deliv Rev* 2013;**65**:104–20.
6. Anselmo AC, Mitragotri S. An overview of clinical and commercial impact of drug delivery systems. *J Control Release* 2014;**190**:15–28.
7. Ma P, Mumper RJ. Paclitaxel nano-delivery systems: a comprehensive review. *J Nanomed Nanotechnol* 2013;**4**:1000164.
8. Meyer RA, Sunshine JC, Green JJ. Biomimetic particles as therapeutics. *Trends Biotechnol* 2015;**33**:514–24.
9. Sleep D. Albumin and its application in drug delivery. *Expert Opin Drug Deliv* 2015;**12**:793–812.
10. Merlot AM, Kalinowski DS, Richardson DR. Unraveling the mysteries of serum albumin—more than just a serum protein. *Front Physiol* 2014;**5**:299.
11. Chen Q, Liang C, Wang C, Liu Z. An imagable and photothermal "abraxane-like" nanodrug for combination cancer therapy to treat subcutaneous and metastatic breast tumors. *Adv Mater* 2015;**27**:903–10.
12. Liu L, Bi Y, Zhou M, Chen X, He X, Zhang Y, et al. Biomimetic human serum albumin nanoparticle for efficiently targeting therapy to metastatic breast cancers. *ACS Appl Mater Interfaces* 2017;**9**:7424–35.
13. Li C, Li Y, Gao Y, Wei N, Zhao X, Wang C, et al. Direct comparison of two albumin-based paclitaxel-loaded nanoparticle formulations: is the crosslinked version more advantageous?. *Int J Pharm* 2014;**468**:15–25.
14. Shao K, Ding N, Huang S, Ren S, Zhang Y, Kuang Y, et al. Smart nanodevice combined tumor-specific vector with cellular microenvironment-triggered property for highly effective antiglioma therapy. *ACS Nano* 2014;**8**:1191–203.
15. Jiang L, Xu Y, Liu Q, Tang Y, Ge L, Zheng C, et al. A nontoxic disulfide bond reducing method for lipophilic drug-loaded albumin nanoparticle preparation: formation dynamics, influencing factors and formation mechanisms investigation. *Int J Pharm* 2013;**443**:80–6.
16. Guo Y, Zhang Y, Li J, Zhang Y, Lu Y, Jiang X, et al. Cell microenvironment-controlled antitumor drug releasing-nanomicelles for GLUT1-targeting hepatocellular carcinoma therapy. *ACS Appl Mater Interfaces* 2015;**7**:5444–53.
17. Zhao S, Wang W, Huang Y, Fu Y, Cheng Y. Paclitaxel loaded human serum albumin nanoparticles stabilized with intermolecular disulfide bonds. *Medchemcomm* 2014;**5**:1658–63.
18. Dipl-Biol KL, Wacker M, Wagner S, Langer K, Von Briesen H. Targeted human serum albumin nanoparticles for specific uptake in EGFR-expressing colon carcinoma cells. *Nanomedicine* 2011;**7**:454–63.
19. Qi WW, Yu HY, Guo H, Lou J, Wang ZM, Liu P, et al. Doxorubicin-loaded glycyrrhetinic acid modified recombinant human serum albumin nanoparticles for targeting liver tumor chemotherapy. *Mol Pharm* 2015;**12**:675–83.
20. Xu R, Fisher M, Juliano RL. Targeted albumin-based nanoparticles for delivery of amphipathic drugs. *Bioconjug Chem* 2011;**22**:870–8.
21. Muñoz M, Coveñas R, Esteban F, Redondo M. The substance P/NK-1 receptor system: NK-1 receptor antagonists as anti-cancer drugs. *J Biosci* 2015;**40**:441–63.
22. Liu Y, He X, Kuang Y, An S, Wang C, Guo Y, et al. A bacteria deriving peptide modified dendrigraft poly-L-lysines (DGL) self-assembling nanoplatform for targeted gene delivery. *Mol Pharm* 2014;**11**:3330–41.
23. Gong G, Xu Y, Zhou Y, Meng Z, Ren G, Zhao Y, et al. Molecular switch for the assembly of lipophilic drug incorporated plasma protein nanoparticles and *in vivo* image. *Biomacromolecules* 2012;**13**:23–8.
24. Wang W, Huang Y, Zhao S, Shao T, Cheng Y. Human serum albumin (HSA) nanoparticles stabilized with intermolecular disulfide bonds. *Chem Commun* 2013;**49**:2234–6.
25. Gu G, Gao X, Hu Q, Kang T, Liu Z, Jiang M, et al. The influence of the penetrating peptide iRGD on the effect of paclitaxel-loaded MT1-AF7p-conjugated nanoparticles on glioma cells. *Biomaterials* 2013;**34**:5138–48.
26. Fukano H, Takahashi T, Aizawa M, Yoshimura H. Synthesis of uniform and dispersive calcium carbonate nanoparticles in a protein cage through control of electrostatic potential. *Inorg Chem* 2011;**50**:6526–32.
27. Shmakov SN, Pinkhassik E. Simultaneous templating of polymer nanocapsules and entrapped silver nanoparticles. *Chem Commun* 2010;**46**:7346–8.
28. De Jong WH, Borm PJ. Drug delivery and nanoparticles: applications and hazards. *Int J Nanomed* 2008;**3**:133–49.
29. Singh AS, Caplan A, Corcoran KE, Fernandez JS, Preziosi M, Rameshwar P. Oncogenic and metastatic properties of preprotachykinin-I and neurokinin-1 genes. *Vasc Pharmacol* 2006;**45**:235–42.
30. Helms HC, Abbott NJ, Burek M, Cecchelli R, Couraud PO, Deli MA, et al. *In vitro* models of the blood-brain barrier: an overview of commonly used brain endothelial cell culture models and guidelines for their use. *J Cereb Blood Flow Metab* 2016;**36**:862–90.
31. Byeon HJ, Thao LQ, Lee S, Min SY, Lee ES, Shin BS, et al. Doxorubicin-loaded nanoparticles consisted of cationic-and mannose-modified-albumins for dual-targeting in brain tumors. *J Control Release* 2016;**225**:301–13.
32. Lin T, Zhao P, Jiang Y, Tang Y, Jin H, Pan Z, et al. Blood–brain-barrier-penetrating albumin nanoparticles for biomimetic drug delivery *via* albumin-binding protein pathways for antiglioma therapy. *ACS Nano* 2016;**10**:9999–10012.
33. Lee JH, Na K, Song SC, Lee J, Kuh HJ. The distribution and retention of paclitaxel and doxorubicin in multicellular layer cultures. *Oncol Rep* 2012;**27**:995–1002.
34. Stehle G, Sinn H, Wunder A, Schrenk HH, Stewart JC, Hartung G, et al. Plasma protein (albumin) catabolism by the tumor itself—implications for tumor metabolism and the genesis of cachexia. *Crit Rev Oncol Hematol* 1997;**26**:77–100.
35. Merlot AM, Kalinowski DS, Richardson DR. Unraveling the mysteries of serum albumin-more than just a serum protein. *Front Physiol* 2014;**5**:299.